


Cite this: *RSC Adv.*, 2018, 8, 5740

# Synthesis of Cu<sub>2</sub>O–CuFe<sub>2</sub>O<sub>4</sub> microparticles from Fenton sludge and its application in the Fenton process: the key role of Cu<sub>2</sub>O in the catalytic degradation of phenol

Muhammad Faheem, Xinbai Jiang,\* Lianjun Wang and Jinyou Shen \*

This paper presents the key role of Cu<sub>2</sub>O in Fenton catalysis using Cu<sub>2</sub>O–CuFe<sub>2</sub>O<sub>4</sub> magnetic microparticles, which were prepared using Fenton sludge as an iron source. The catalytic activity of the as-prepared Cu<sub>2</sub>O–CuFe<sub>2</sub>O<sub>4</sub> and CuFe<sub>2</sub>O<sub>4</sub> microparticles was evaluated in a heterogeneous Fenton system for the degradation of recalcitrant phenol. The Cu<sub>2</sub>O–CuFe<sub>2</sub>O<sub>4</sub> microparticles demonstrated relatively superior catalytic performance as compared to CuFe<sub>2</sub>O<sub>4</sub> microparticles when used as a Fenton catalyst. The relatively higher catalytic activity of Cu<sub>2</sub>O–CuFe<sub>2</sub>O<sub>4</sub> for phenol degradation during the Fenton process could be attributed to the availability of both monovalent [Cu(I)] and divalent [Cu(II)] as well as Fe(II)/Fe(III) redox pairs, which could react quickly with H<sub>2</sub>O<sub>2</sub> to generate hydroxyl radicals (HO<sup>•</sup>). An electron bridge was formed between Cu(I) and Fe(III), which accelerates the formation of Fe(II) species in order to boost the reaction rate. Highly reactive and excessively available Cu(I) species for as prepared Cu<sub>2</sub>O–CuFe<sub>2</sub>O<sub>4</sub> microparticles could be considered to be rather crucial for the generation of highly reactive HO<sup>•</sup> radical species. In addition, the as-prepared Cu<sub>2</sub>O–CuFe<sub>2</sub>O<sub>4</sub> magnetic microparticles exhibited sound stability and reusability.

Received 23rd December 2017  
Accepted 30th January 2018

DOI: 10.1039/c7ra13608k

rsc.li/rsc-advances

## 1. Introduction

Fenton oxidation technology, which is well known as advanced oxidation processes (AOPs), has been extensively used to remove various recalcitrant or non-biodegradable organic pollutants from industrial wastewater.<sup>1,2</sup> During Fenton process, a powerful oxidant, hydroxyl radicals (HO<sup>•</sup>) can be generated efficiently at near-ambient temperature and pressure by the reaction between Fe<sup>2+</sup> and H<sub>2</sub>O<sub>2</sub>.<sup>3</sup> The distinct properties of generated hydroxyl radicals (HO<sup>•</sup>) such as strong oxidation potential ( $E^0 = 2.8$  V) and non-selective reactivity are considered to be responsible for the effectiveness of AOPs in the field of organic pollutant elimination. These generated radicals can react with a variety of organic pollutants, causing efficient degradation, even complete mineralization.<sup>4,5</sup> However, in spite of the simplicity of Fenton process, bulk quantity of iron sludge generated during neutralization after Fenton oxidation restricts its implementation on large scale due to the increasing cost for Fenton sludge treatment and disposal to avoid environment deterioration.<sup>6</sup>

Two approaches have been implemented to reduce the Fenton sludge generation yield, *i.e.*, development of

heterogeneous iron bearing catalyst and reuse of Fenton sludge as iron source. Various heterogeneous catalysts have been synthesized, such as nano scale zero-valent iron,<sup>7</sup> iron-containing clays,<sup>8</sup> natural minerals,<sup>9</sup> iron exchanged zeolite,<sup>10</sup> and some solid support immobilized by iron.<sup>11,12</sup> Immobilization of iron within the interlayer of heterogeneous catalysts results in relatively high oxidation performance. Moreover, heterogeneous catalysts have been proven to be superior to classical homogeneous catalysts *i.e.*, Fe<sup>2+</sup>, because they are easily separated from wastewater treatment system through applied magnetic field or simple sedimentation. Yoo *et al.*, suggested the recycling of iron incorporated sludge produced in Fenton oxidation system as coagulant during coagulation process.<sup>13</sup> Through the recycling of Fenton sludge as coagulant, coagulant dosage could be lowered by 50% and sludge disposal could be decreased by 50%. Recycling of iron incorporated sludge also follows the 3R's rules regarding integrated solid waste management, *i.e.*, reduce, reuse and recycle. Iron sludge-graphene composite with low amount of graphene were synthesized as a heterogeneous Fenton catalyst by using iron sludge as the iron precursor. The as-prepared catalyst showed wide pH operating range, excellent stability, and was efficient for the degradation of acid red G and metronidazole.<sup>14</sup> Zhang *et al.* synthesized magnetic biochar catalyst by using ferric sludge and biological sludge *via* hydrothermal process. This catalyst showed excellent characteristics to promote a heterogeneous Fenton reaction in methylene blue treatment.<sup>15</sup> These

Jiangsu Key Laboratory of Chemical Pollution Control and Resources Reuse, School of Environmental and Biological Engineering, Nanjing University of Science and Technology, Nanjing 210094, Jiangsu Province, China. E-mail: xinbai\_jiang@njust.edu.cn; shenjinyou@mail.njust.edu.cn; Fax: +86 25 84315941; +86 25 84303965; Tel: +86 25 84315941; +86 25 84303965



methods hold promise for ferric sludge waste reclamation and heterogeneous Fenton catalyst fabrication.

In addition to the recycling of iron incorporated sludge, the use of low cost heterogeneous catalyst in Fenton treatment could be another alternative for the reduction of hazardous ferric sludge. Recently, different approaches have been investigated to boost up the performance of synthesized heterogeneous Fenton catalyst, *e.g.*, to reduce the catalyst size up to nano-scale in order to increase surface energy and available active sites, to embed appropriate transition metal (Cu, Ni, V, Ti, Cr, Zn, Mn and Co, *etc.*) into the skeleton of  $\text{Fe}_3\text{O}_4$  to improve the catalyst performance.<sup>16</sup> The improvement of heterogeneous catalyst performance as a result of transition metals embedment into  $\text{Fe}_3\text{O}_4$  structure could be attributed to the synergetic effect between newly inserted transition metal and  $\text{Fe}^{3+}$ . This synergetic effect could be described by formation of galvanic cell between embedded transition metal and  $\text{Fe}^{3+}$ . The improvement in catalyst activity could be ascribed to formation of redox pairs  $\text{Fe}^{3+}/\text{Fe}^{2+}$  due to rapid electron flow as a result of transition metal insertion into  $\text{Fe}_3\text{O}_4$  structure. A newly developed material can be implemented in different fields if it holds the properties of higher reactivity, sound stability and easy separation from reaction medium.

Mixed iron oxides or ferrites have drawn much more attention of scientist and researcher due to their ability to apply in different fields such as microwave devices,<sup>17</sup> catalysis or catalyst,<sup>18</sup> magnetic fluids<sup>19</sup> and gas sensors.<sup>20</sup> Recently, various ferrites such as  $\text{ZnFe}_2\text{O}_4$  (ref. 21) and  $\text{CuFe}_2\text{O}_4$ ,<sup>22</sup> and iron-copper bimetallic nanoparticles embedded within ordered mesoporous carbon composite,<sup>23</sup> have been utilized as the catalyst for heterogeneous Fenton like process to remove organic contaminants from wastewater. In our previous study,  $\text{NiFe}_2\text{O}_4$  were synthesized through co-precipitation method followed by sintering at 800 °C.<sup>24</sup> In the Fenton system using  $\text{NiFe}_2\text{O}_4$  as heterogeneous catalyst, phenol removal efficiency as high as  $95 \pm 3.4\%$  could be achieved, indicating excellent catalytic performance of  $\text{NiFe}_2\text{O}_4$  in the heterogeneous Fenton process. Roonasi and Nezhad carried out a comparative study to investigate the performance of synthetic M-ferrite nanoparticles (M = Cu, Zn, Fe or Mn) in heterogeneous catalysis. Among these ferrite nanoparticles,  $\text{CuFe}_2\text{O}_4$  was found to be the best catalyst for phenol removal, as 78% of 100 mg L<sup>-1</sup> phenol could be efficiently removed within 175 min.<sup>25</sup> In addition, the effectiveness of Cu(I) species as compare to Cu(II) species for the activation of  $\text{H}_2\text{O}_2$  in order to generate  $\text{HO}^\bullet$  radicals for the degradation of bisphenol has been confirmed in literature.<sup>26</sup> Recently, the nanocomposite  $\text{CuO-CuFe}_2\text{O}_4$  has been synthesized in a single stage by one pot polyol method. The electrical, structural and optical properties of the synthesized  $\text{CuO-CuFe}_2\text{O}_4$  were investigated as a function of different annealing temperatures ranges from 200–1000 °C.<sup>27</sup> Furthermore, a novel and recyclable magnetic catalyst  $\text{Cu}_2\text{O/nano-CuFe}_2\text{O}_4$  has been reported for the coupling of carbonyl compounds–alkynes–amines in order to synthesize propargylamines under solvent-free condition.<sup>28</sup> These studies gave us a direction to synthesize  $\text{Cu}_2\text{O-CuFe}_2\text{O}_4$  particles with both Cu(I) and Cu(II) species, resulting in the fast activation of  $\text{H}_2\text{O}_2$  to get hydroxyl radicals

$\text{HO}^\bullet$  for the elimination of recalcitrant organic pollutant such as phenol.

In this study, we have explored a facile and novel method to fabricate  $\text{Cu}_2\text{O-CuFe}_2\text{O}_4$  microparticles using Fenton sludge as iron source, which was further used as a heterogeneous catalyst in Fenton process for the elimination of recalcitrant phenol. Thus, the aims of the present study were (1) to fabricate and characterize  $\text{Cu}_2\text{O-CuFe}_2\text{O}_4$ , (2) to assess the catalytic activity of fabricated  $\text{Cu}_2\text{O-CuFe}_2\text{O}_4$  in Fenton oxidation, (3) to investigate the synergetic effect of Cu(I)/Cu(II) as well as Fe(III)/Fe(II) redox pairs in Fenton reaction, and (4) to propose possible catalytic mechanism involved in efficient Fenton reaction at the presence of  $\text{Cu}_2\text{O-CuFe}_2\text{O}_4$ .

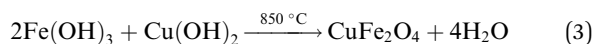
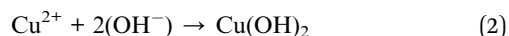
## 2. Materials and methods

### 2.1 Characteristics of the Fenton sludge used

The characteristics of iron-containing sludge obtained from neutralization process after Fenton oxidation could be described as follows. As a rich iron source, total iron content of Fenton sludge used for the synthesis of Fenton catalyst was as high as  $8.65 \pm 0.78 \text{ g L}^{-1}$ . Chemical oxygen demand (COD) concentration of the Fenton sludge used was about  $6700 \pm 375 \text{ mg L}^{-1}$ . The higher COD value exhibited the presence of abundant organics in Fenton sludge. Moreover, the Fenton sludge used in this study could be fluidized in nature, having total solid as well as water content of about  $87.48\% \pm 0.97\%$  and  $12.52 \pm 0.97\%$ , respectively.

### 2.2 Synthesis of $\text{CuFe}_2\text{O}_4$ microparticles

$\text{CuFe}_2\text{O}_4$  microparticles were prepared by co-precipitation technique, *i.e.*,  $\text{CuSO}_4 \cdot 5\text{H}_2\text{O}$  was dissolved into ultrapure water and then the prepared  $\text{CuSO}_4$  solution was mixed with Fenton sludge at Fe/Cu molar ratio of 2 : 1. Thereafter, sodium hydroxide solution ( $5 \text{ mol L}^{-1}$ ) was added into the mixture of Fenton sludge and  $\text{CuSO}_4$  drop by drop under continuous stirring to raise the pH value to 10.0. The mixture was stirred continuously at temperature of 65 °C for 2 h. The obtained precipitate was then separated by centrifugation and washed with ultrapure water until the pH value of the filtrate reached 7.0. The resulting product was kept in an oven at temperature of 105 °C for 3 h to make it dry and then finally sintered at 850 °C for 3 h under nitrogen atmosphere. The formation of  $\text{CuFe}_2\text{O}_4$  microparticles could be described by eqn (1)–(3):

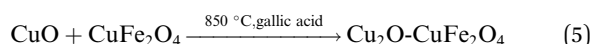
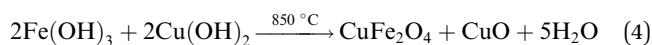


### 2.3 Synthesis of $\text{Cu}_2\text{O-CuFe}_2\text{O}_4$ microparticles

$\text{Cu}_2\text{O-CuFe}_2\text{O}_4$  microparticles were prepared through modified hydrothermal technique.<sup>29</sup> In this case,  $\text{CuSO}_4 \cdot 5\text{H}_2\text{O}$  solution and Fenton sludge were mixed together at Fe/Cu molar ratio of



1 : 1. Sodium hydroxide solution (5 mol L<sup>-1</sup>) was added drop wise into the mixture of Fenton sludge and CuSO<sub>4</sub> under continuous stirring to raise the pH value to 10.0 to get colloidal suspension. After this, 0.97 g gallic acid was blended with the suspension. The obtained mixture was sonicated for 15 min and then was poured into a 200 mL Teflon-line stainless steel autoclave. The closed autoclave was then allowed to keep at 200 °C for almost 12 h and finally cooled normally to room temperature. During hydrothermal process the gallic acid attached with chemical substances as organic ligands. The obtained product was separated and washed several times with ultrapure water, then dried at 105 °C and finally sintered at 850 °C for 3 h under nitrogen atmosphere. The calcination temperature was chosen as 850 °C because higher temperature causes lower reactivity and lower temperature favors severe leaching from catalysts.<sup>30</sup> Moreover, for comparison purpose, the Cu<sub>2</sub>O microparticles was synthesized in a similar way by using CuSO<sub>4</sub>·5H<sub>2</sub>O individually as a precursor material. The formation of Cu<sub>2</sub>O–CuFe<sub>2</sub>O<sub>4</sub> microparticles could be described by eqn (4) and (5):



## 2.4 Catalytic degradation experiment

Catalytic degradation of phenol was carried out in a series of 100 mL centrifuge tubes. 50 mL phenol solution at initial concentration of 250 mg L<sup>-1</sup> and initial pH of 4.0 was added into these centrifuge tubes. Fenton reaction was initiated by adding H<sub>2</sub>O<sub>2</sub> and magnetic heterogeneous Fenton catalyst into phenol solution. The initial concentration of H<sub>2</sub>O<sub>2</sub> and magnetic heterogeneous Fenton catalyst was set at 80 mmol L<sup>-1</sup> and 2 g L<sup>-1</sup>, respectively. The Fenton reaction was carried out on a rotary shaker at 30 °C and 220 rpm. The heterogeneous Fenton catalyst was recovered from solution after the reaction by applying external magnetic field for expected reuse. The control experiments carried out with Fenton catalyst but without H<sub>2</sub>O<sub>2</sub> or with H<sub>2</sub>O<sub>2</sub> but without Fenton catalyst were performed in the same manner.

## 2.5 Characterization and analytical methods

Total iron content of Fenton sludge, copper and iron leaching were analyzed through Inductive Couple Plasma Optical Emission Spectrometer (ICP-OES) (Optima 7000DV, PerkinElmer, USA). A mixture of 2.5 mL HClO<sub>4</sub>, 2.5 mL HNO<sub>3</sub> (69%) and 10 mL HF (40%) was used for wet digestion of Fenton sludge. The COD concentration of Fenton sludge was analyzed by the standard potassium dichromate method. SEM (JSM-6380, JEOL, Japan) and HRTEM (FEI Philips CM300 UT/FEG) were applied to characterize the surface morphology, size and shape of as prepared CuFe<sub>2</sub>O<sub>4</sub> and Cu<sub>2</sub>O–CuFe<sub>2</sub>O<sub>4</sub> microparticles. BET (Micromeritics, ASAP 2020, USA) surface area was quantified by nitrogen adsorption data at 77 K. For the investigation of crystal structure of as-prepared materials, XRD (D8 Advance, Burker,

Germany) analysis was performed. X-Ray Photoelectron Spectroscopy (XPS, ESCALAB 250) technique was implemented to determine the synthesized materials elemental composition and different oxidation states of corresponding elements. The magnetic strength was tested on a vibrating sample magnetometer (VSM) (Lake Shore 7410, Lake Shore Cryotronics, Inc. USA). Phenol identification and quantification was carried out by high performance liquid chromatography (HPLC) (Waters 2996, Waters Incorporation, USA). Identification of intermediates formed during phenol degradation was confirmed by GC-MS as well as HPLC.

# 3. Results and discussion

## 3.1 Characterization of the synthesized microparticles

In this study, the CuFe<sub>2</sub>O<sub>4</sub> and Cu<sub>2</sub>O–CuFe<sub>2</sub>O<sub>4</sub> microparticles were synthesized by co-precipitation and modified hydrothermal method followed by sintering under nitrogen atmosphere. Fig. 1 showed the SEM and high resolution TEM images of CuFe<sub>2</sub>O<sub>4</sub> and Cu<sub>2</sub>O–CuFe<sub>2</sub>O<sub>4</sub> microparticles. It was obvious that only one type of specific shape agglomerated particles could be observed in case of synthesized CuFe<sub>2</sub>O<sub>4</sub> microparticles (Fig. 1(a)). However, for Cu<sub>2</sub>O–CuFe<sub>2</sub>O<sub>4</sub> microparticles, two different types of agglomerated particles could be observed and the new types of agglomerated particles were pointed out with red arrows in SEM image (Fig. 1(b)). Similar evidence was revealed by high resolution TEM images (Fig. 1(c) and (d)). Two different particles were existed in case of Cu<sub>2</sub>O–CuFe<sub>2</sub>O<sub>4</sub> microparticles as compared to CuFe<sub>2</sub>O<sub>4</sub> microparticles, the results were in agreement with SEM images. Through comparison between both synthesized particles and literature review, it was speculated that the microparticles with the shape like chrysanthemum might be Cu<sub>2</sub>O, which should be further clarified by XRD analysis. The Cu/Cu<sub>2</sub>O/CuO@C catalyst particles recently synthesized by Zhao *et al.*, which had excellent catalytic performance, was also similar to chrysanthemum as in our case.<sup>31</sup> BET surface area analysis was also carried out for the synthesized heterogeneous catalysts, as indicated in Table 1. The BET surface area (1.08 m<sup>2</sup> g<sup>-1</sup>) for CuFe<sub>2</sub>O<sub>4</sub> particles was smaller than that of Cu<sub>2</sub>O–CuFe<sub>2</sub>O<sub>4</sub> particles (1.65 m<sup>2</sup> g<sup>-1</sup>), which might be directed towards the generation of additional chrysanthemum shaped Cu<sub>2</sub>O particles along with CuFe<sub>2</sub>O<sub>4</sub> particles at the presence of gallic acid. The presence of puffy ball-like structure particles might result in higher BET surface area of Cu<sub>2</sub>O–CuFe<sub>2</sub>O<sub>4</sub> particles. For synthesized Cu<sub>2</sub>O micro particles the BET surface area was 1.50 m<sup>2</sup> g<sup>-1</sup> which was higher than that of CuFe<sub>2</sub>O<sub>4</sub> (1.08 m<sup>2</sup> g<sup>-1</sup>). It could be referred to puffy ball like shape of Cu<sub>2</sub>O particles.

XRD analysis was carried out to examine the crystal phase and structure of synthesized products (Fig. 2). The diffraction peaks appeared at 2θ of 18.5° (111), 30.2° (220), 35.6° (311), 37.2° (222), 43.0° (400), 57.1° (511), 62.8° (440) and 74.5° (533) could be assigned to pure cuprospinel CuFe<sub>2</sub>O<sub>4</sub> (JCPDS#25-0283). In comparison with pure cuprospinel CuFe<sub>2</sub>O<sub>4</sub>, newly originated diffraction peaks positioning at 2θ of 36.7° (111), 42.5° (200), 61.6° (220) and 73.7° (311) could be attributed to rhombic dodecahedral crystal of Cu<sub>2</sub>O (JCPDS#05-0667) in





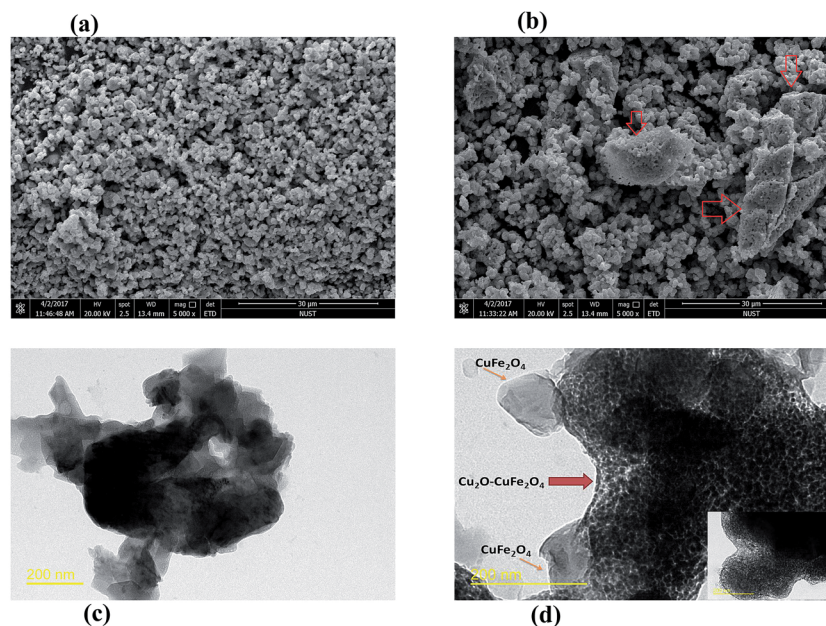


Fig. 1 SEM (a, b) and high resolution TEM (c, d) images of  $\text{CuFe}_2\text{O}_4$  and  $\text{Cu}_2\text{O-CuFe}_2\text{O}_4$ .

cubic phase, which confirmed the existence of  $\text{Cu}_2\text{O}$  in as-synthesized  $\text{Cu}_2\text{O-CuFe}_2\text{O}_4$ .

XPS technique was applied for thorough study of chemical composition and different oxidation states of constituent elements of synthesized materials. From XPS wide spectrum in Fig. 3(a), it was clear that both microparticles were comprised of same parent constituents, such as Fe, Cu and O elements. Someone could differentiate between materials having the same parent constituents on the behalf of different oxidation states of existed constituent elements. For example, existence of  $\text{Cu}^{2+}$  in  $\text{CuFe}_2\text{O}_4$  and the presence of  $\text{Cu}^+$  in  $\text{Cu}_2\text{O-CuFe}_2\text{O}_4$  materials could be confirmed on the behalf of different binding energy of  $\text{Cu}^{2+}$  and  $\text{Cu}^+$ , respectively. As shown in Fig. 3(b), the detail XPS spectra of Cu 2p reveals that strong  $\text{Cu}^{2+}$  satellites could be observed at binding energy of 942.5 eV and 962.5 eV along with peak at 934.3 eV, which confirmed the presence of  $\text{Cu}^{2+}$  in  $\text{CuFe}_2\text{O}_4$ .<sup>32,33</sup> In addition, on the basis of the relatively weak peak at 932.1 eV,<sup>34</sup> there were  $\text{Cu}^+$  species on the surface of  $\text{CuFe}_2\text{O}_4$ , which might come from the reduction of  $\text{Cu}^{2+}$  during calcination process due to the abundant organics in Fenton sludge. In contrast, for  $\text{Cu}_2\text{O-CuFe}_2\text{O}_4$ , there was a relatively strong peak at 932.1 eV in Fig. 3(c), which could be referred to  $\text{Cu}_2\text{O}$ . Similar result was found for  $\text{Cu/Cu}_2\text{O/CuO@C}$  catalyst particles.<sup>31</sup> In addition, peak at 934.3 eV and weak satellite peaks at 942.5 eV and 962.5 eV confirm the

formation of  $\text{Cu}^{2+}$  along with  $\text{CuFe}_2\text{O}_4$  particles for as-prepared  $\text{Cu}_2\text{O-CuFe}_2\text{O}_4$  microparticles. Moreover, for wide scan of Fe 2p spectra, the peaks raised at 711.4 eV along with shakeup satellite pointed at 719.9 eV corresponded to the existence of  $\text{Fe}^{3+}$  cations. However, XPS spectrum for Fe 2p and O 1s for both  $\text{CuFe}_2\text{O}_4$  and  $\text{Cu}_2\text{O-CuFe}_2\text{O}_4$  were similar, as shown in Fig. 3(a) and (d).

The magnetic property of the as-prepared  $\text{Cu}_2\text{O-CuFe}_2\text{O}_4$  and  $\text{CuFe}_2\text{O}_4$  was determined by applied field of  $\pm 10\,000$  Oe. As shown in Fig. (4), the saturation magnetization and coercivity values for as-prepared  $\text{Cu}_2\text{O-CuFe}_2\text{O}_4$  and  $\text{CuFe}_2\text{O}_4$  were  $71\text{ emu g}^{-1}$  and  $73\text{ Oe}$ ,  $61\text{ emu g}^{-1}$  and  $50\text{ Oe}$ , respectively. The magnetic hysteresis loop exhibited better ferromagnetic behavior of  $\text{Cu}_2\text{O-CuFe}_2\text{O}_4$  as compared to  $\text{CuFe}_2\text{O}_4$ . The material having magnetic features could be easily separated by external applied magnetic field for possible reuse.  $\text{CuFe}_2\text{O}_4$  nanoparticles synthesized by Phuruangrat *et al.* through microwave-hydrothermal method showed a maximum saturation magnetization of about  $56\text{ emu g}^{-1}$ .<sup>35</sup> Higher saturation magnetization values of  $\text{Cu}_2\text{O-CuFe}_2\text{O}_4$  observed in this study could be attributed to the presence of additional  $\text{Cu}_2\text{O}$  in  $\text{CuFe}_2\text{O}_4$  particles. Previous study about the magnetic property of  $\text{Cu}_2\text{O}$  has confirmed that  $\text{Cu}_2\text{O}$  could act as a diamagnetic to ferromagnetic depending upon the role of native defects in bulk  $\text{Cu}_2\text{O}$ .<sup>36</sup>

Table 1 Catalyst or catalysts physicochemical properties, their catalytic performance and metals ions leaching

Catalyst	BET S. area ( $\text{m}^2\text{ g}^{-1}$ )	Average particle size ( $\mu\text{m}$ )	TOC removal (%)	Phenol removal (%)	Iron leaching ( $\text{mg L}^{-1}$ )	Copper leaching ( $\text{mg L}^{-1}$ )
$\text{CuFe}_2\text{O}_4$	1.08	2–3	$47.6 \pm 1.0$	$57.8 \pm 3.6$	1.16	30.18
$\text{Cu}_2\text{O-CuFe}_2\text{O}_4$	1.65	0.5–2	$85.6 \pm 0.7$	$97.2 \pm 0.4$	1.53	28.60
$\text{Cu}_2\text{O}$	1.50	2–3.5	$36.5 \pm 1.5$	$61.9 \pm 2.3$	—	—



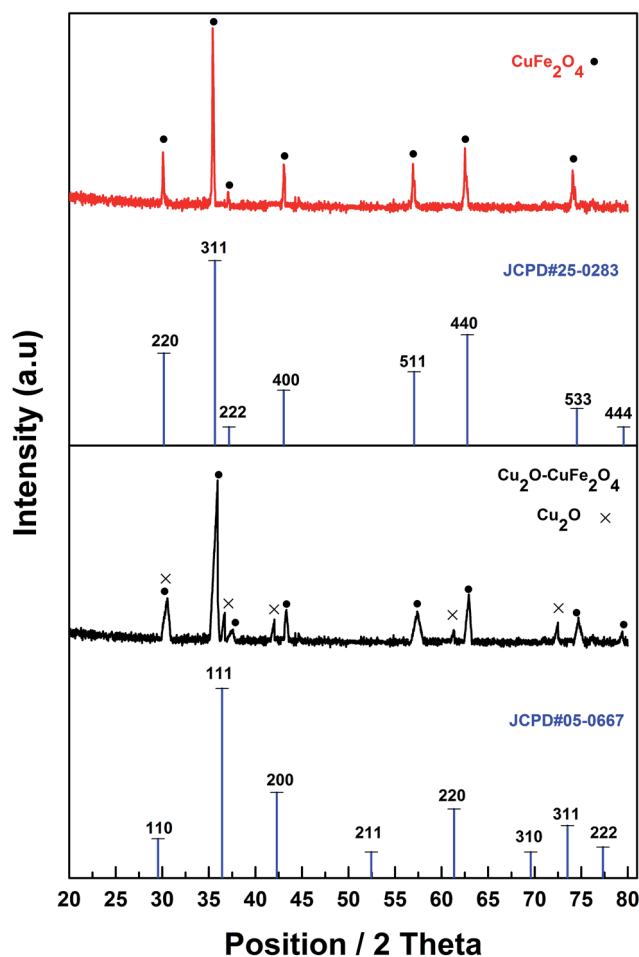


Fig. 2 XRD of  $\text{CuFe}_2\text{O}_4$  and  $\text{Cu}_2\text{O}-\text{CuFe}_2\text{O}_4$ .

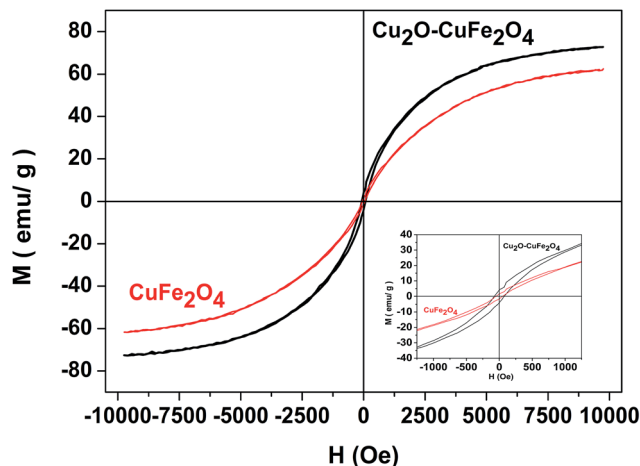


Fig. 4 Hysteresis curve for  $\text{Cu}_2\text{O}-\text{CuFe}_2\text{O}_4$  and  $\text{CuFe}_2\text{O}_4$ .

### 3.2 Heterogeneous Fenton performance of $\text{Cu}_2\text{O}-\text{CuFe}_2\text{O}_4$

Heterogeneous Fenton performance of the catalyst prepared was mainly dependent on the potential to generate hydroxyl radical ( $\text{OH}^\bullet$ ) through  $\text{H}_2\text{O}_2$  decomposition. As shown in Fig. 5(a), in the system with  $\text{H}_2\text{O}_2$  alone but without  $\text{CuFe}_2\text{O}_4$  or  $\text{Cu}_2\text{O}-\text{CuFe}_2\text{O}_4$ , phenol removal efficiency within 60 min was as low as  $6.4 \pm 0.6\%$ , indicating the poor oxidation ability of  $\text{H}_2\text{O}_2$  alone toward phenol. In the control experiments without  $\text{H}_2\text{O}_2$  but with  $\text{CuFe}_2\text{O}_4$  and  $\text{Cu}_2\text{O}-\text{CuFe}_2\text{O}_4$ , phenol removal efficiencies were  $11.4 \pm 1.7\%$  and  $13.8 \pm 1.0\%$ , respectively, which could be attributed to the adsorption of phenol by as-prepared  $\text{CuFe}_2\text{O}_4$  and  $\text{Cu}_2\text{O}-\text{CuFe}_2\text{O}_4$ . When  $\text{CuFe}_2\text{O}_4$  and  $\text{Cu}_2\text{O}$  were utilized in the presence of  $\text{H}_2\text{O}_2$ , phenol removal efficiency within 60 min was significantly increased to  $57.8 \pm 3.6\%$  and

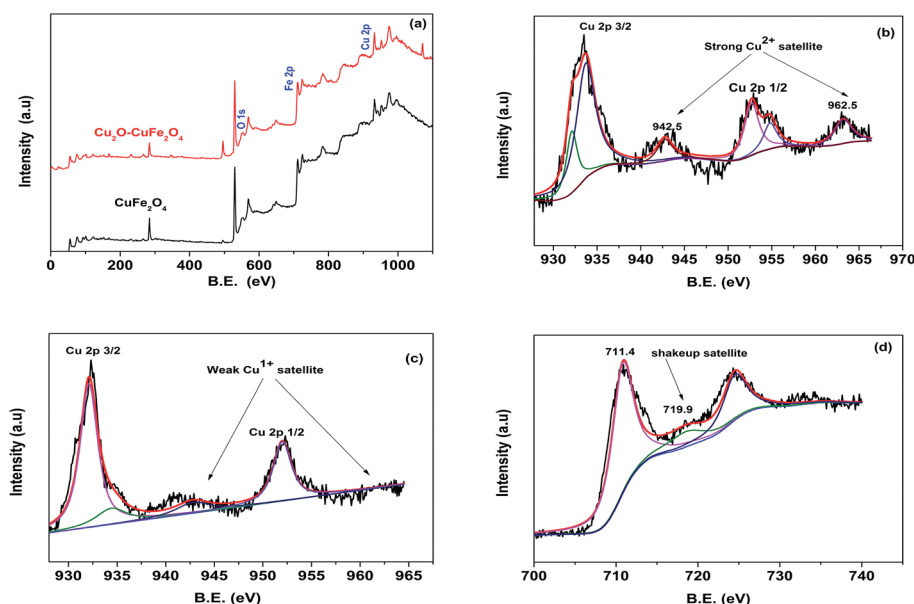


Fig. 3 XPS spectra for  $\text{CuFe}_2\text{O}_4$  and  $\text{Cu}_2\text{O}-\text{CuFe}_2\text{O}_4$  (a), strong  $\text{Cu}^{2+}$  satellite for  $\text{CuFe}_2\text{O}_4$  (b), weak  $\text{Cu}^{1+}$  satellite for  $\text{Cu}_2\text{O}-\text{CuFe}_2\text{O}_4$  (c), similar Fe 2p region for both  $\text{CuFe}_2\text{O}_4$  and  $\text{Cu}_2\text{O}-\text{CuFe}_2\text{O}_4$  (d).



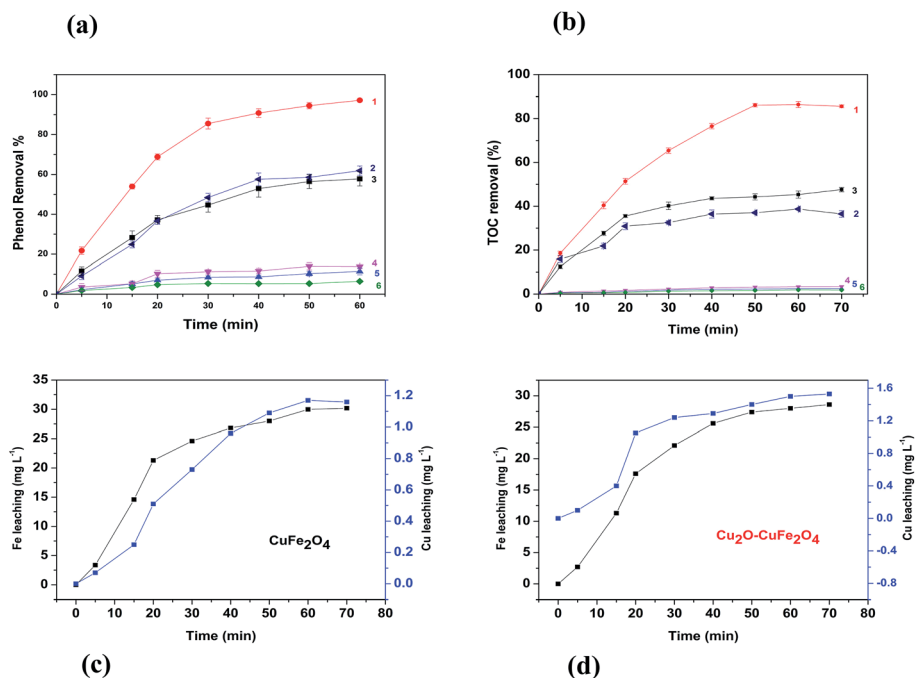


Fig. 5 Catalysts performance for phenol removal (a), TOC removal (b), iron and copper leaching for CuFe<sub>2</sub>O<sub>4</sub> (c) and Cu<sub>2</sub>O-CuFe<sub>2</sub>O<sub>4</sub> (d). (1): Cu<sub>2</sub>O-CuFe<sub>2</sub>O<sub>4</sub> + H<sub>2</sub>O<sub>2</sub>; (2): Cu<sub>2</sub>O + H<sub>2</sub>O<sub>2</sub>; (3): CuFe<sub>2</sub>O<sub>4</sub> + H<sub>2</sub>O<sub>2</sub>; (4): Cu<sub>2</sub>O-CuFe<sub>2</sub>O<sub>4</sub> alone; (5) CuFe<sub>2</sub>O<sub>4</sub> alone; (6) H<sub>2</sub>O<sub>2</sub> alone.

61.9 ± 2.3%, respectively, indicating the positive role of CuFe<sub>2</sub>O<sub>4</sub> and Cu<sub>2</sub>O in phenol oxidation by H<sub>2</sub>O<sub>2</sub>. In case of Cu<sub>2</sub>O, slightly higher phenol removal efficiency as compared to CuFe<sub>2</sub>O<sub>4</sub> could be attributed to more active site availability due to higher surface area and relatively more generation of HO· radical than HO<sub>2</sub>· as a result of monovalent copper Cu(I). Moreover, When Cu<sub>2</sub>O-CuFe<sub>2</sub>O<sub>4</sub> was used as Fenton catalyst, phenol removal efficiency increased sharply within 30 min to 85.5 ± 2.8% and further increased to 97.2 ± 0.4% within 60 min. When Cu<sub>2</sub>O-CuFe<sub>2</sub>O<sub>4</sub> was used as the catalyst for phenol oxidation by H<sub>2</sub>O<sub>2</sub>, a remarkable increase in terms of phenol removal indicated better catalysis performance of Cu<sub>2</sub>O-CuFe<sub>2</sub>O<sub>4</sub> than CuFe<sub>2</sub>O<sub>4</sub> and Cu<sub>2</sub>O.

Moreover, TOC removal observed in heterogeneous Fenton system followed the similar trend. As indicated in Fig. 5(b), in the Fenton system with H<sub>2</sub>O<sub>2</sub> alone, with CuFe<sub>2</sub>O<sub>4</sub> alone and with Cu<sub>2</sub>O-CuFe<sub>2</sub>O<sub>4</sub> alone, TOC removal efficiencies within 60 min were as low as 1.8 ± 0.1%, 2.5 ± 0.1%, 3.4 ± 0.1%, respectively. However, in Fenton system catalyzed by Cu<sub>2</sub>O, CuFe<sub>2</sub>O<sub>4</sub>, and Cu<sub>2</sub>O-CuFe<sub>2</sub>O<sub>4</sub>, TOC removal efficiencies within 60 min were as high as 36.5 ± 1.5%, 47.6 ± 1.0% and 85.6 ± 0.7%, respectively. Nevertheless, no remarkable increase of TOC removal efficiencies could be observed when reaction time prolonged to 70 min. TOC removal performance confirmed the amazing catalytic activity of CuFe<sub>2</sub>O<sub>4</sub> and Cu<sub>2</sub>O-CuFe<sub>2</sub>O<sub>4</sub> towards H<sub>2</sub>O<sub>2</sub> oxidation, especially for Cu<sub>2</sub>O-CuFe<sub>2</sub>O<sub>4</sub>.

Fenton and Cu<sup>2+</sup> coupled system has been studied for the enhanced mineralization of phenol, with phenol removal efficiency as high as 94% was achieved in Fenton-Cu<sup>2+</sup> system at initial phenol concentration of 100 mg L<sup>-1</sup>.<sup>24,37</sup> In addition, Stoia *et al.* prepared MnFe<sub>2</sub>O<sub>4</sub> nanoparticles, which was used for

the oxidative degradation of phenol at initial concentration of about 50 mg L<sup>-1</sup>.<sup>38</sup> Phenol removal efficiency of 90% could be achieved at pH of 3.0–3.5 under the catalyst dosage of 3 g L<sup>-1</sup>. In this study, phenol removal efficiency as high as 97.2 ± 0.4% could be achieved within 60 min at the presence of Cu<sub>2</sub>O-CuFe<sub>2</sub>O<sub>4</sub>, even at initial phenol concentration as high as 250 mg L<sup>-1</sup>. The relatively higher catalytic role of Cu<sub>2</sub>O-CuFe<sub>2</sub>O<sub>4</sub> obtained in this study could be attributed to the coexistence of both monovalent copper [Cu(I)] and divalent copper [Cu(II)] in the structure of Cu<sub>2</sub>O-CuFe<sub>2</sub>O<sub>4</sub>.

### 3.3 Sound stability and reusability of Cu<sub>2</sub>O-CuFe<sub>2</sub>O<sub>4</sub>

Leaching study for the as-prepared CuFe<sub>2</sub>O<sub>4</sub> and Cu<sub>2</sub>O-CuFe<sub>2</sub>O<sub>4</sub> was carried out to investigate their stability and reusability, as shown in Fig. 5(c) and (d). The concentration of leached iron at pH 4.0 for CuFe<sub>2</sub>O<sub>4</sub> and Cu<sub>2</sub>O-CuFe<sub>2</sub>O<sub>4</sub> was 30.18 mg L<sup>-1</sup> and 28.60 mg L<sup>-1</sup>, accounted for 3.22% and 4.77% of the total iron contents at applied catalyst dosage of 2.0 g L<sup>-1</sup>. Moreover, for CuFe<sub>2</sub>O<sub>4</sub> and Cu<sub>2</sub>O-CuFe<sub>2</sub>O<sub>4</sub>, the observed copper leaching was 1.16 mg L<sup>-1</sup> and 1.53 mg L<sup>-1</sup>, accounted for 0.22% and 0.15% of total copper contents at applied catalyst dosage of 2.0 g L<sup>-1</sup>. Although the iron leaching for Cu<sub>2</sub>O-CuFe<sub>2</sub>O<sub>4</sub> was a little higher than that of CuFe<sub>2</sub>O<sub>4</sub>, the observed copper leaching for Cu<sub>2</sub>O-CuFe<sub>2</sub>O<sub>4</sub> was lower than that of CuFe<sub>2</sub>O<sub>4</sub>. Therefore, Cu<sub>2</sub>O-CuFe<sub>2</sub>O<sub>4</sub> microparticles show good stability as compared to CuFe<sub>2</sub>O<sub>4</sub> considering the low leaching of copper. In addition, these values for iron and copper leaching observed in this study were relatively lower than those reported in the literature. For example, the iron leaching accounted for 5.08% of the total iron contents at applied catalyst dosage of 0.24 g L<sup>-1</sup> has been



reported in literature, where ferrite particles were applied as heterogeneous Fenton catalyst for the degradation of Rhodamine B.<sup>39</sup> Fontecha-Cámara *et al.* applied mixed iron oxide as Fenton catalyst in order to remove gallic acid from aqueous solutions.<sup>40</sup> The observed copper leaching for copper ferrite was  $2.85 \text{ mg L}^{-1}$  at pH 4.3, which accounted for 21.50% of the total copper contents at applied catalyst dosage of  $0.05 \text{ g L}^{-1}$ . As for the reusability,  $\text{Cu}_2\text{O}-\text{CuFe}_2\text{O}_4$  exhibited a slight decrease in phenol degradation efficiency (from  $97.2 \pm 0.4\%$  to  $85.7 \pm 0.5\%$ ) within five consecutive runs, as shown in Fig. 6(a). However, in case of  $\text{CuFe}_2\text{O}_4$ , a sharp decrease of phenol removal efficiency (from  $57.77 \pm 3.55\%$  to  $32.32 \pm 1.55\%$ ) was observed even after three cycles, as indicated in Fig. 6(b). The decrease in phenol degradation efficiency was due to vanishing of available active site on  $\text{CuFe}_2\text{O}_4$  surface after reuse, which could be overcome through the incorporation of  $\text{Cu}_2\text{O}$  in  $\text{CuFe}_2\text{O}_4$  structure.

### 3.4 The possible mechanism involved in Fenton reaction by $\text{Cu}_2\text{O}-\text{CuFe}_2\text{O}_4$

Based on the above results, the possible mechanism involved in Fenton reaction by  $\text{Cu}_2\text{O}-\text{CuFe}_2\text{O}_4$  could be described in Fig. 7. In our case, the available  $\text{Fe}(\text{III})$  on both  $\text{CuFe}_2\text{O}_4$  and  $\text{Cu}_2\text{O}-\text{CuFe}_2\text{O}_4$  surface was firstly reduced into  $\text{Fe}(\text{II})$  due to its reaction with adsorbed  $\text{H}_2\text{O}_2$  on the surface of both microparticles. The desired  $\text{HO}^\bullet$  radical was produced when the generated  $\text{Fe}(\text{II})$  further reacted with  $\text{H}_2\text{O}_2$  in a similar way, which was known as

Haber-Weiss process.<sup>41</sup> Literature study reveals that conversion of  $\text{Fe}(\text{III})$  to  $\text{Fe}(\text{II})$  was very slow when compared with the conversion of  $\text{Fe}(\text{II})$  to  $\text{Fe}(\text{III})$ .<sup>42</sup> The presence of transition metal copper in the skeleton of spinel catalyst may enhance phenol degradation due to availability of  $\text{Cu}(\text{II})/\text{Cu}(\text{I})$  redox pairs, which causes acceleration of the redox cycle of  $\text{Fe}(\text{III})/\text{Fe}(\text{II})$  ions at room temperature. Zhang *et al.* prepared  $\text{CuFe}_2\text{O}_4$  microparticles for the degradation of bisphenol A, confirming the effectiveness of  $\text{Cu}(\text{I})$  species as compare to  $\text{Cu}(\text{II})$  species for the activation of  $\text{H}_2\text{O}_2$  to generate  $\text{HO}^\bullet$  radicals.<sup>26</sup> As indicated in literature study, the reaction rate constant ( $k$ ) between monovalent copper [ $\text{Cu}(\text{I})$ ] and  $\text{H}_2\text{O}_2$  was as high as  $1.0 \times 10^4 \text{ M}^{-1} \text{ s}^{-1}$ , as compared to that between divalent copper [ $\text{Cu}(\text{II})$ ] and  $\text{H}_2\text{O}_2$ , which was as low as  $4.6 \times 10^2 \text{ M}^{-1} \text{ s}^{-1}$ .<sup>43</sup> In our study, the generation of reactive  $\text{HO}^\bullet$  radical may start by ligand displacement between the hydrous surface of  $\text{Fe}^{\text{III}}-\text{OH}/\text{Cu}^{\text{II}}-\text{OH}$  and  $\text{H}_2\text{O}_2$ , with the generation of  $\text{Fe}^{\text{III}}\cdot\text{H}_2\text{O}_2$  and  $\text{Cu}^{\text{II}}\cdot\text{H}_2\text{O}_2$ . Then initially generated  $\text{Fe}^{\text{III}}\cdot\text{H}_2\text{O}_2$  and  $\text{Cu}^{\text{II}}\cdot\text{H}_2\text{O}_2$  species can produce  $\text{HO}_2^\bullet$  and regenerate  $\text{Fe}^{\text{II}}$  and  $\text{Cu}^{\text{I}}$  by intramolecular electron transfer, which subsequently produced  $\text{HO}^\bullet$  and degraded phenol. The hydroxyl radicals  $\text{HO}^\bullet$  were considered as major oxidizing species for phenol mineralization and  $\text{HO}_2^\bullet$  radicals as minor oxidizing species. The generation route for major and minor oxidizing species, and proposed mechanism for phenol degradation could be described by eqn (6)–(15):

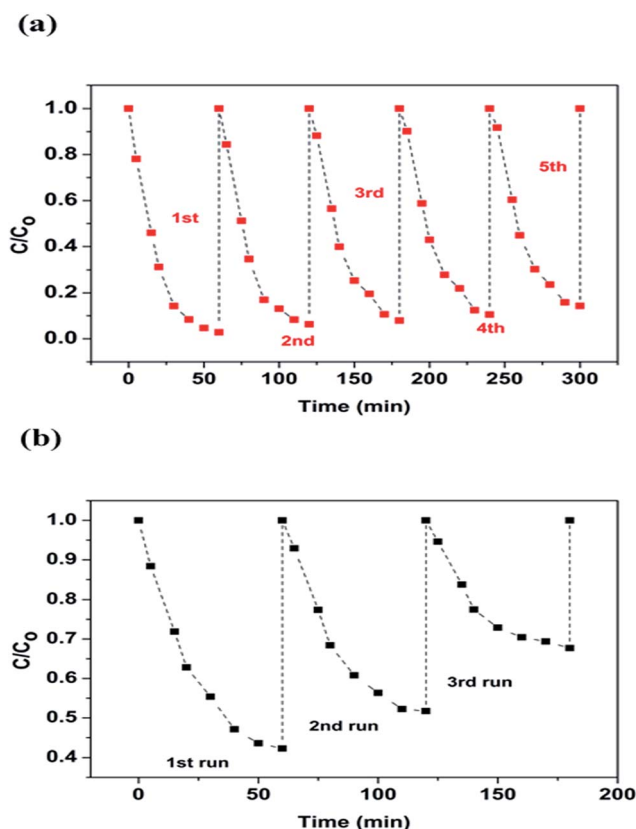
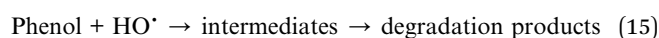
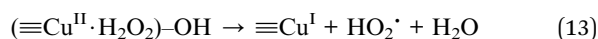
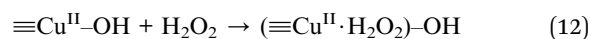
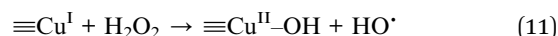
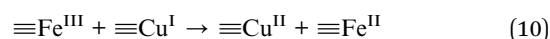
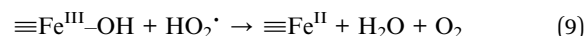
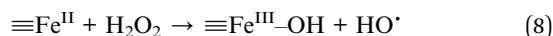
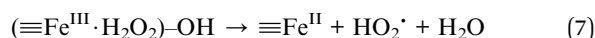
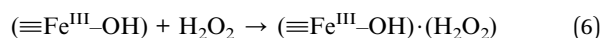


Fig. 6 Reusability study for  $\text{Cu}_2\text{O}-\text{CuFe}_2\text{O}_4$  (a) and  $\text{CuFe}_2\text{O}_4$  (b).

The higher degradation efficiency of phenol for the as-prepared  $\text{Cu}_2\text{O}-\text{CuFe}_2\text{O}_4$  could be attributed to the presence of both monovalent copper [ $\text{Cu}(\text{I})$ ] and divalent copper [ $\text{Cu}(\text{II})$ ]. The existence of redox pairs  $\text{Cu}(\text{I})/\text{Cu}(\text{II})$  is likely considered as the key source for the activation of  $\text{H}_2\text{O}_2$  in order to generate  $\text{HO}^\bullet$  radicals. The coexistence of  $\text{Cu}(\text{I})$  and  $\text{Cu}(\text{II})$  in  $\text{Cu}_2\text{O}-\text{CuFe}_2\text{O}_4$  resulted in faster reaction with  $\text{H}_2\text{O}_2$  as compared to  $\text{CuFe}_2\text{O}_4$  microparticles containing divalent copper [ $\text{Cu}(\text{II})$ ] alone in the structure. The faster reaction might be due to rapid electron ( $e^-$ ) transfer or formation of galvanic cell or electron bridge between [ $\text{Cu}(\text{I})$ ] and  $\text{Fe}(\text{III})$  along with the





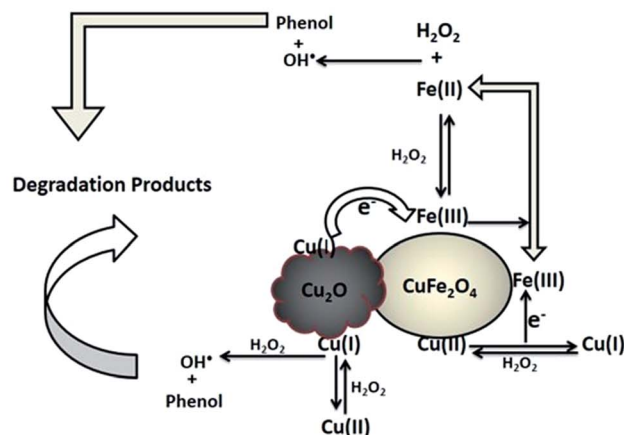
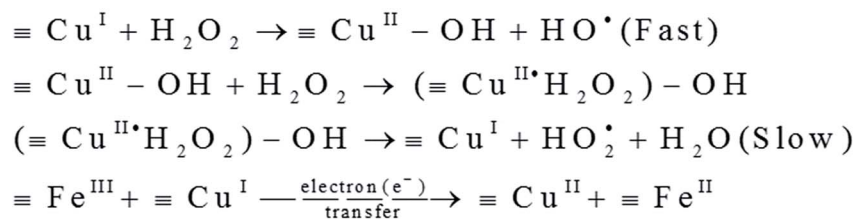


Fig. 7 Possible mechanisms for phenol degradation in Fenton system based on  $\text{Cu}_2\text{O}-\text{CuFe}_2\text{O}_4$ .

production of highly reactive radical  $\text{HO}^\bullet$  as compared to  $\text{HO}_2^\bullet$  species. For the mineralization of carbamazepine, Ding *et al.* prepared recyclable  $\text{CuFeO}_2$  microparticles for heterogeneous activation of peroxymonosulfate (PMS) in order to generate sulfate radicals ( $\text{SO}_4^{\bullet-}$ ). It was concluded that enhanced activation of PMS by micro- $\text{CuFeO}_2$  referred to synergetic effect of surface  $\text{Cu}(\text{I})$  and  $\text{Fe}(\text{III})$ .<sup>44</sup> The higher Fenton activity by  $\text{Cu}_2\text{O}-\text{CuFe}_2\text{O}_4$  might also be attributed to faster reaction rate between  $\text{Cu}(\text{I})$  and  $\text{H}_2\text{O}_2$  due to presence of additional  $\text{Cu}_2\text{O}$  particles, which results in faster reduction of  $\text{H}_2\text{O}_2$  in order to generate highly reactive radical species  $\text{HO}^\bullet$ . The faster reduction of  $\text{H}_2\text{O}_2$  due to presence of  $\text{Cu}_2\text{O}$  additional particles in case of  $\text{Cu}_2\text{O}-\text{CuFe}_2\text{O}_4$  microparticles causes the relatively efficient consumption of  $\text{H}_2\text{O}_2$  due to more available and highly reactive  $\text{Cu}(\text{I})$  species.

## 4. Conclusion

The present work focus on the synthesis of a heterogeneous Fenton catalyst, namely  $\text{Cu}_2\text{O}-\text{CuFe}_2\text{O}_4$ , for the reuse of iron incorporated in Fenton sludge. In comparison to  $\text{CuFe}_2\text{O}_4$ , much higher phenol catalytic degradation was found for  $\text{Cu}_2\text{O}-\text{CuFe}_2\text{O}_4$ , indicating the key role of  $\text{Cu}_2\text{O}$  in Fenton reaction. The rapid electron transfer built up galvanic cell between  $\text{Cu}(\text{I})$  and  $\text{Fe}(\text{III})$ , which favored the formation of relatively excess  $\text{Fe}(\text{II})$  species. The highly reactive  $\text{Fe}(\text{II})$  species interaction with adsorbed  $\text{H}_2\text{O}_2$  gave abundant  $\text{HO}^\bullet$  radicals for phenol degradation. The higher Fenton catalytic activity of  $\text{Cu}_2\text{O}-\text{CuFe}_2\text{O}_4$  could be attributed to the synergetic effect between  $\text{Cu}(\text{I})/\text{Cu}(\text{II})$  and  $\text{Fe}(\text{II})/\text{Fe}(\text{III})$  redox pairs. The as prepared  $\text{Cu}_2\text{O}-\text{CuFe}_2\text{O}_4$  was stable, recoverable and reusable, offering a promising potential as a heterogeneous Fenton catalyst.

## Conflicts of interest

There are no conflicts of interest to declare.

## Acknowledgements

This research is financed by Natural Science Foundation of Jiangsu Province for Distinguished Young Scholars (BK20170038), National Natural Science Foundation of China (51708293) and Natural Science Foundation of Jiangsu Province (BK20170842).

## References

- 1 J. Xu, Y. Long, D. Shen, H. Feng and T. Chen, *J. Hazard. Mater.*, 2017, **323**, 674–680.
- 2 D. Gümüş and F. Akbal, *Process Saf. Environ. Prot.*, 2016, **103**, 252–258.
- 3 J. He, X. Yang, B. Men and D. Wang, *J. Environ. Sci.*, 2016, **39**, 97–109.
- 4 W. M. Wang, J. Song and X. Han, *J. Hazard. Mater.*, 2013, **262**, 412–419.
- 5 E. Mousset, L. Frunzo, G. Esposito, E. D. van Hullebusch, N. Oturan and M. A. Oturan, *Appl. Catal., B*, 2016, **180**, 189–198.
- 6 X. J. Ma and H. L. Xia, *J. Hazard. Mater.*, 2009, **162**, 386–390.
- 7 Y. Li, Y. Zhang, J. Li and X. Zheng, *Environ. Pollut.*, 2011, **159**, 3744–3749.
- 8 J. Feng, X. Hu, P. L. Yue and S. Qiao, *Sep. Purif. Technol.*, 2009, **67**, 213–217.
- 9 E. Garrido-Ramírez, B. Theng and M. Mora, *Appl. Clay Sci.*, 2010, **47**, 182–192.





- 10 M. Tekbaş, H. C. Yatmaz and N. Bektaş, *Microporous Mesoporous Mater.*, 2008, **115**, 594–602.
- 11 M. Aleksić, H. Kušić, N. Koprivanac, D. Leszczynska and A. L. Božić, *Desalination*, 2010, **257**, 22–29.
- 12 W. Wang, M. Zhou, Q. Mao, J. Yue and X. Wang, *Catal. Commun.*, 2010, **11**, 937–941.
- 13 H.-C. Yoo, S.-H. Cho and S.-O. Ko, *J. Environ. Sci. Health, Part A: Environ. Sci. Eng.*, 2001, **36**, 39–48.
- 14 S. Guo, N. Yuan, G. Zhang and J. C. Yu, *Microporous Mesoporous Mater.*, 2017, **238**, 62–68.
- 15 H. Zhang, G. Xue, H. Chen and X. Li, *Chemosphere*, 2018, **191**, 64–71.
- 16 R. C. Costa, M. d. F. F. Lelis, L. C. Oliveira, J. D. Fabris, J. D. Ardisson, R. R. Rios, C. N. Silva and R. M. Lago, *Catal. Commun.*, 2003, **4**, 525–529.
- 17 T. Giannakopoulou, L. Kompotiatis, A. Kontogeorgakos and G. Kordas, *J. Magn. Magn. Mater.*, 2002, **246**, 360–365.
- 18 M. Rashad and O. Fouad, *Mater. Chem. Phys.*, 2005, **94**, 365–370.
- 19 E. Hasmonay, J. Depeyrot, M. Sousa, F. Tourinho, J.-C. Bacri, R. Perzynski, Y. L. Raikher and I. Rosenman, *J. Appl. Phys.*, 2000, **88**, 6628–6635.
- 20 N. Rezlescu, N. Iftimie, E. Rezlescu, C. Doroftei and P. Popa, *Sens. Actuators, B*, 2006, **114**, 427–432.
- 21 F. Zhang, C. Wei, Y. Hu and H. Wu, *Sep. Purif. Technol.*, 2015, **156**, 625–635.
- 22 Y. Ding, L. Zhu, S. Wang and H. Tang, *Appl. Catal., B*, 2013, **129**, 153–162.
- 23 Y. Wang, H. Zhao and G. Zhao, *Appl. Catal., B*, 2015, **164**, 396–406.
- 24 H. Zhang, J. Liu, C. Ou, Faheem, J. Shen, H. Yu, Z. Jiao, W. Han, X. Sun, J. Li and L. Wang, *J. Environ. Sci.*, 2017, **53**, 1–8.
- 25 P. Roonasi and A. Y. Nezhad, *Mater. Chem. Phys.*, 2016, **172**, 143–149.
- 26 X. Zhang, Y. Ding, H. Tang, X. Han, L. Zhu and N. Wang, *Chem. Eng. J.*, 2014, **236**, 251–262.
- 27 K. Ramachandran, S. Chidambaram, B. Baskaran, A. Muthukumarasamy and G. M. Kumar, *Mater. Lett.*, 2016, **175**, 106–109.
- 28 F. Nemat, A. Elhampour, H. Farrokhi and M. B. Natanzi, *Catal. Commun.*, 2015, **66**, 15–20.
- 29 X. Qiu, M. Liu, K. Sunada, M. Miyauchi and K. Hashimoto, *Chem. Commun.*, 2012, **48**, 7365–7367.
- 30 J. Du, J. Bao, X. Fu, C. Lu and S. H. Kim, *Sep. Purif. Technol.*, 2016, **11**, 145–152.
- 31 X. Zhao, Y. Tan, F. Wu, H. Niu, Z. Tang, Y. Cai and J. P. Giesy, *Sci. Total Environ.*, 2016, **571**, 380–387.
- 32 L. Huang, F. Peng and F. S. Ohuchi, *Surf. Sci.*, 2009, **603**, 2825–2834.
- 33 Z. Ai, L. Zhang, S. Lee and W. Ho, *J. Phys. Chem. C*, 2009, **113**, 20896–20902.
- 34 C. D. Wagner and G. Muilenberg, *Handbook of X-ray photoelectron spectroscopy*, Perkin-Elmer, 1979.
- 35 A. Phuruangrat, B. Kuntalue, S. Thongtem and T. Thongtem, *Mater. Lett.*, 2016, **167**, 65–68.
- 36 X. Yu, X. Zhang, S. Wang and G. Feng, *Curr. Appl. Phys.*, 2015, **15**, 1303–1311.
- 37 J. Maekawa, K. Mae and H. Nakagawa, *J. Environ. Chem. Eng.*, 2014, **2**, 1275–1280.
- 38 M. Stoia, C. Muntean and B. Militaru, *J. Environ. Sci.*, 2016, **53**, 269–277.
- 39 T. R. Giraldo, C. C. Arruda, G. M. da Costa, E. Longo and C. Ribeiro, *J. Sol-Gel Sci. Technol.*, 2009, **52**, 299–303.
- 40 M. A. Fontecha-Cámara, C. Moreno-Castilla, M. V. López-Ramón and M. A. Álvarez, *Appl. Catal., B*, 2016, **196**, 207–215.
- 41 S.-S. Lin and M. D. Gurol, *Environ. Sci. Technol.*, 1998, **32**, 1417–1423.
- 42 K. Li, Y. Zhao, M. J. Janik, C. Song and X. Guo, *Appl. Surf. Sci.*, 2017, **396**, 1383–1392.
- 43 A. D. Bokare and W. Choi, *J. Hazard. Mater.*, 2014, **275**, 121–135.
- 44 Y. Ding, H. Tang, S. Zhang, S. Wang and H. Tang, *J. Hazard. Mater.*, 2016, **317**, 686–694.

